submitted to Diamond Films '92/ICNDST-3, Heidelberg Sept. 1992

DEVICE PROPERTIES OF HOMOEPITAXIALLY GROWN DIAMOND

M. I. Landstrass, M. A. Plano, M. A. Moreno and S. McWilliams
Crystallume, 125 Constitution Drive, Menlo Park CA 94025 (U.S.A.)

L. S. Pan, D. R. Kania, and S. Han
Lawrence Livermore National Laboratory, L-476, 7000 East Avenue, Livermore, CA 94550 (U.S.A)

Abstract

Homoepitaxial single crystal diamond layers were grown on naturally occurring type Ia and type IIa gemstone diamond substrates using microwave plasma assisted CVD deposition techniques. The epitaxial layers ranged in thickness from 0.5μm to 800μm. Single crystals were grown both unintentionally doped and intentionally doped by means of gas phase dopants. Planar photoconductive diodes were fabricated from the high resistivity crystals and junction diodes were fabricated from the boron doped crystal layers. The photoconductive diode response was measured and the output signals were analyzed to derive the carrier mobility and lifetime. Combined carrier photoconductive mobility values exceeded 3500cm^2/V-s only seen in the best IIa gemstone diamonds. Junction diodes yielded the highest breakdown fields with typical values in excess of 2x10^7 V/cm dielectric strength.

1. Introduction

The development of processes and equipment for the routine deposition of chemical vapor deposited (CVD) diamond has started development efforts aimed towards the

incorporation of these films into all areas of the electronics industry[1-9]. Technological advancements leading to electronic applications of diamond films are closely linked to the evolution of diamond film quality. Single crystal diamond grown using CVD techniques offers the opportunity to achieve the highest quality possible with this technology.

Devices fabricated from homoepitaxial diamond should exceed the performance of comparable gemstone diamond devices with respect to carrier mobility and dielelectric breakdown strength. One of the major issues in the growth of high quality single crystal diamond by CVD is the choice of a suitable substrate. While economic constraints make inexpensive substrates such as silicon desirable, heteroepitaxial growth technology for diamond is currently nonexistent. We desire fabrication techniques that allow for the growth of low defect single crystal diamond independent of the substrate. In the present work techniques for the homoepitaxial CVD growth of diamond on diamond susbstrates is investigated and the affect of substrate choice is discussed.

2. Experimental Details

Homoepitaxial single crystal diamond layers were grown on naturally occurring type Ia and type IIa gemstone diamond substrates using microwave plasma assisted CVD deposition techniques. The substrates, purchased from Dubbledee-Harris, were polished and aligned with a (100) orientation and were 1 mm x 1 mm x 100μm, 2 mm x 2 mm x 250μm and 4 mm x 4mm x 250μm. Microwave power at 2.45 GHz is coupled into the CVD reactor chamber through waveguides where a standing wave of TE10 mode is established. The reactor was equiped with gas sources and flow controllers for argon, hydrogen, methane, oxygen, carbon monoxide, phosphine and diborane. Typical reactor conditions were a pressure of 60 Torr and a power of 2kW. The gemstone diamond substrates were solvent degreased before growth and loaded into the reactor on silicon

holders. The holder temperature was monitored by an optical pyrometer which indicated nominal growth temperatures of 800°C. Significant temperature variations could exist due to the proximity of the substrate to the plasma. The epitaxial layers grown ranged in thickness from 0.5μm to 800μm and had growth rates of between 2μm/hr to 10μm/hr. The single crystal layers were grown both unintentionally doped and intentionally doped by means of gas phase introduction of diborane or phosphine gas. The homoepitaxial layers were analyzed by angle resolved Raman, X-ray topography and scanning electron microscopy.

Planar photoconductive diodes were fabricated from the higher resistance crystals and junction diodes were fabricated from the more conductive boron doped layers. The steady state photoconductive diode response was measured using a deuterium lamp source and in pulse mode using an ultraviolet laser.

3. Results

Figure 1 is a SEM micrograph showing the growth surface of a 260μm epitaxial layer grown on top of a 4 mm x 4mm x 250μm type IIa substrate. The main feature of this micrograph is the planarity of the epilayer and the lack of secondary nucleation. In this growth the laser cut edge regions, which often act as nucleation sites, were also replicated in the growing film. Only the four corners of the gemstone nucleated uneven or polycrystalline growth. Figure 2 is an optical micrograph of the epilayer pictured in Fig. 1 illustrating the high clarity and low visible light absorption of this layer. From Figs. 1 and 2 it can be seen that there are no polycrystalline inclusions or cracks in the epilayer. Inclusions and cracks are the most significant defects in that they render the diamonds useless as device substrates. The occurrence of these macroscopic defects had no consistent trend with respect to growth conditions but had a strong trend with respect to

substrates. When grown in the same reactor at the same time, inclusions would always occur at higher densities on type Ia gemstones and off orientation crystal faces such as at corners and edges. No consistent dopant related effect on morphology was determined during doping with either phosphine or diborane.

The Raman spectra of the homoepitaxial diamond films showed a narrow diamond peak with a typical full width at half maximum of 2.6 cm^{-1} [10] and no indication of non-diamond bonded carbon. X-ray topographic images of one of the epilayer sample found them to be very similar to the type IIa substrate. It was found however that only poor quality images were possible in both the substrate and the epilayer due to the broad angle diffraction from both the type IIa substrate and the epilayer.

Figure 3 shows a plot of the ultraviolet absorption of epilayers of 100, 260 and 500μm in thickness along with a 250μm thick type IIa gemstone similar to that used as the substrate. From Fig. 3 a broad absorption merged with the band edge occurs in all the epilayers but due to the overall low absorption is only readily detected in the thicker samples. This absorption shows up in the visible as a slight yellow-brown coloration and is not present in the type IIa substrates as received. This absorption may arise from stress in the grown layers. As one of the dominant film defects is cracking, this also suggests that many of the films are stressed. Raman spectra from some of the epilayer samples show well defined shifts indicative of stress[10].

Figure 4 is a SEM micrograph of an interdigitated metal/diamond/metal ultraviolet light photoconductor. The detectors were fabricated by sputtering either Ti/Au or Mo/Au electrodes with no special surface preparation other than solvent cleaning. Before contact deposition the diamond samples were annealed in N_2 at 400°C, no additional anneal was performed prior to measurement. The device active regions defined by the metal,are 35μm

long gaps, 700 μm in width separated by 10μm metal lines. Photoconductor diodes were also fabricated in a stripline configuration. In these devices the metal defines the device, greatly simplifying the device construction. Figure 5 displays the dark and light current-voltage characteristics of the diode of Fig. 4 when illuminated with an unfiltered deuterium lamp. The light signal is approximately 250 times smaller when illuminated with much higher intensity white light with no UV content. This is consistent with the low level sub-bandgap optical absorption data.. No saturation effects were observed for this device up to an applied voltage of 100V corresponding to an average electric field of 2.9×10^4V/cm.

Figures 6 and 7 plot photoconductiviy results measured with a pulsed UV laser operating at 6.1eV. .These plots indicate photocarrier to carrier effects dominating the device performance at high illumination while the materials properties dominate at low light intensities. Also plotted on the same figure are typical results for a type IIa gemstone device. From Figs. 6 and 7 it can be seen that the epilayer materials properties are very comparable to that of type IIa gemstones. The carrier mobilities of $3500 cm^2/VS$ are typical of the best IIa samples while the carrier lifetimes of 220ps. are slightly worse than typical. In order to determine the likely factors controlling the device performance, photoconductor diodes were fabricated from crystals doped with phosphorus and boron. Table 1 lists the results comparing the properties of these diodes as a function of doping. From the gas phase concentrations of 0.9ppm we estimate from previous chemical analysis that the dopant concentrations were approximately $1 \times 10^{17} cm^{-3}$. From Table 1 it is apparent that even low levels of doping give rise to large degradations in the photocarrier transport properties in these devices.

In order to ascertain if the dopants were causing precipitates which resulted in unusual scattering properties, diodes were fabricated from boron doped epilayers grown with higher concentrations of boron. Diodes could not be fabricated from the phosphorus

doped layers due to their high resistance at all doping levels. Due to the conductive nature of the boron doped films an isolation step had to be performed as part of the device processing. Figure 8 is an SEM micrograph showing a 30μm thick boron doped epilayer isolated with a 50μm deep mesa etch. The etch was performed using a reactive ion etch (RIE) reactor and molecular oxygen. In Fig. 8 the top of the mesas are very smooth indicative of an active region with no inclusions. Inclusions always give rise to diodes that very low terminal breakdown field or are shorted. Figure 9 plots the current voltage characteristics of a diode fabricated with a tungsten rectifying contact and gold/molybdenum ohmic contacts. The ohmic contacts were alloyed in H_2 at 900°C followed by a N_2 anneal at 400°C. From the doping level of $1x10^{18}cm^{-3}$ the calculated maximum electric field applied to this device is $2x10^7v/cm$. This high electric field without breakdown indicates that the epilayer is of high quality with very few macroscopic or microscopic defects such as precipitates that cause electric field enhancement leading to low breqkdown voltages.

5. Conclusions

Homoepitaxial CVD diamond was grown with transport and device properties of similar quality to type IIa gemstone diamond. The measurements performed on devices doped with boron and phosphorus suggest that impurity effects control the transport electronic properties of CVD homoepitaxial diamond layers. Recent results on polycrystalline material show comparable carrier mobilities to epitaxial and type IIa gemstone diamond and also suggests that impurities are the dominant defect in CVD diamond. Structural defects of a macroscopic size do preclude diode performance such as is evident in Fig. 9. Functioning junction diodes were free from visible defects. We found no evidence of submicroscopic defects.

Of great interest is the ultimate performance capabilities of diamond devices. The results reported here show that CVD diamon can readily achieve the performance limits of type IIa gemstone diamond. These results suggest that type IIa gemstone diamonds although "fabricated" in an impure environment may not be limited by impurities but by other factors such as stress. The next level of major improvements in CVD diamond will be through the control and reduction of crystal stress.

Acknowledgements

We would like to acknowledge support from the Superconducting Super Collider Laboratory at the DOE , SDIO/IST, and the Army at Ft. Monmouth.

References

1. M. W. Geis, D. D. Rathman, D. J. Ehrlich, R. A. Murphy, and W. T. Lindley, IEEE Dev. Let., 8 341 (1987).

2. M. W. Geis, N. N. Efremow, D. D. Rathman, J. Vac. Sci. Technol., vol. A6, pp. 1953-1954, 1988.

3. M. W. Geis, D. D. Rathman, J.J. Zavhowski, D. Smyth, D. K. Smith and G. A. Ditmer, 1988 3rd ONR Diamond Technology Initiative Symp. Abs. (Crystal City, Va.) pp115-8.

4. M. C. Hicks, C. R. Wronski, S. A. Grot, G. Sh. Gildenblat, A. R. Badzian, T. Badzian and R. Messier, J. Appl. Phys. 65 2139 (1989).

5. M. I. Landstrass and K. V. Ravi, Proceedings. of the Fourth International High Frequency Power Conversion Conference, Naples, Fl. (Intertec Communications, Ventura, 1989) p. 103.

6. M. I. Landstrass and D. M. Fleetwood, Appl. Phys. Lett. 56, June 4(1990)

7. H. Shiomi, Y. Nishibayashi, and N. Fujimori, JAPS Conf. Abstract, Fall 1989.

8. N. Fujimori, T. Imai, and A. Doi, Vacuum 36 99 (1986)

9. K. Okano, H. Naruki, Y. Akiba, T. Kurosu, M. Iida, Y. Hirose, and T. Nakamura, JJAP **28** 1066 (1989).

10. H. Herchen, M. A. Cappelli, M. I. Landstrass, M. A. Plano, and M. D. Moyer, Thin Solid Films, **212** 206 (1992)

11. L. S. Pan, S. Han, D. R. Kania, M. A. Plano, M. I. Landstrass, this volume

Figure Captions

Figure 1. Scanning electron micrograph of a 260μm thick epitaxial layer grown on top of a type IIa gemstone diamond of dimensions 4mm x 4mm x 250μm.

Figure 2. Optical micrograph of a 260 micron thick diamond epitaxial layer grown on top of a 4x4mm type IIa diamond 250 micron in thickness.

Figure 3. Ultraviolet transmission near the the band edge of a gemstone type IIa diamond 250μm in thickness plotted along transmission curves for diamond epitaxial layers of thicknesses 100, 260, and 500μm. The epitaxial layers were deposited on type IIa diamond 250μm in thickness.

Figure 4. Scanning electron micrograph of an interdigitated metal/diamond/metal ultraviolet light photoconductor. The device active regions are 35 μm long gaps, 700 microns in width separated by 10μm wide metal lines.

Figure 5 Current-voltage characteristics of the diode pictured in Fig. 4. The traces were measured with the sample shielded from light and with the diode irradiated using an unfiltered deuterium discharge lamp. At 100V the device field was 2.9 x 10^4V/cm. The device response to visible light from a tungsten lamp of much higher power was 250 times less than the signal from the deuterium lamp.

Figure 6. Photoconductivity mobility versus carrier density as adjusted by modulating the UV light intensity of 6.1eV pulsed laser. The solid lines are theoretical fits using the experimental low carrier density mobility and photocarrier to photocarrier induced

scattering. The dots are the epitaxial layer sample and the squares are a type IIa natural diamond. The mobility values of both samples are very close.

Figure 7. Epitaxial diamond and natural diamond photoconductor diode lifetime versus carrier density as adjusted by modulating the UV light intensity of 6.1eV pulsed laser. The lower curve in this figure is the epilayer device.

Figure 8. Scanning electron micrograph of a boron doped diamond epitaxial layer processed through the device mesa isolation step designed to isolate adjacent devices. The mesa etching was performed using RIE etching with molecular oxygen feed gas. The susbstrate had dimensions of 1mm x 1mm x 100μm.

Figure 9. A plot of the forward and reverse voltage characteristics of a junction diode fabricated from a boron doped epilayer using tungsten metallization and measured at 298K and 647K.

Table 1. Effects of doping on photoconductor properties

Dopant	Gas Phase Concentration and Species	Photocarrier lifetime (ps)	Combined mobility (cm^2/V-s)
undoped		220	3500
phosphorus	0.9ppm phosphine	85	500
Boron	0.9ppm diborane	90	200

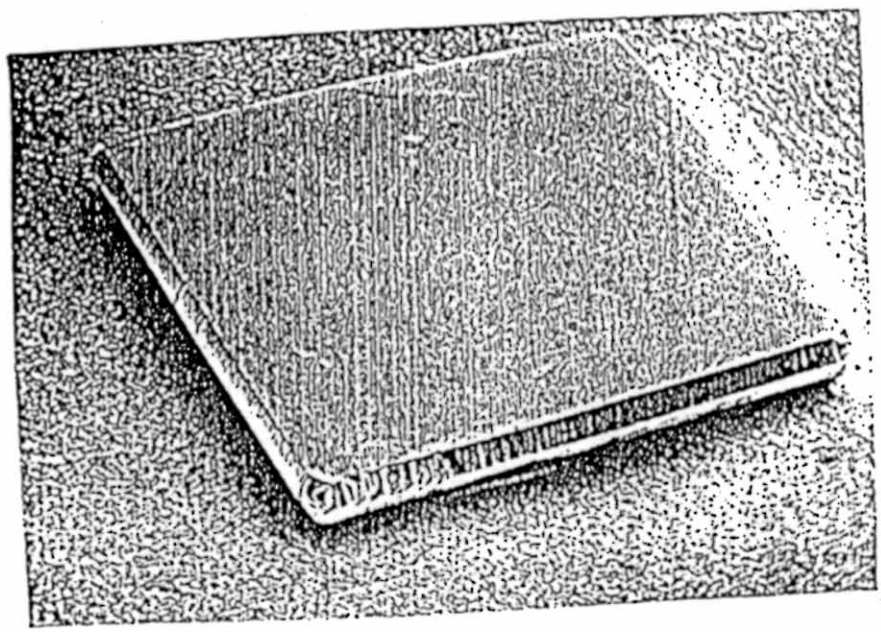

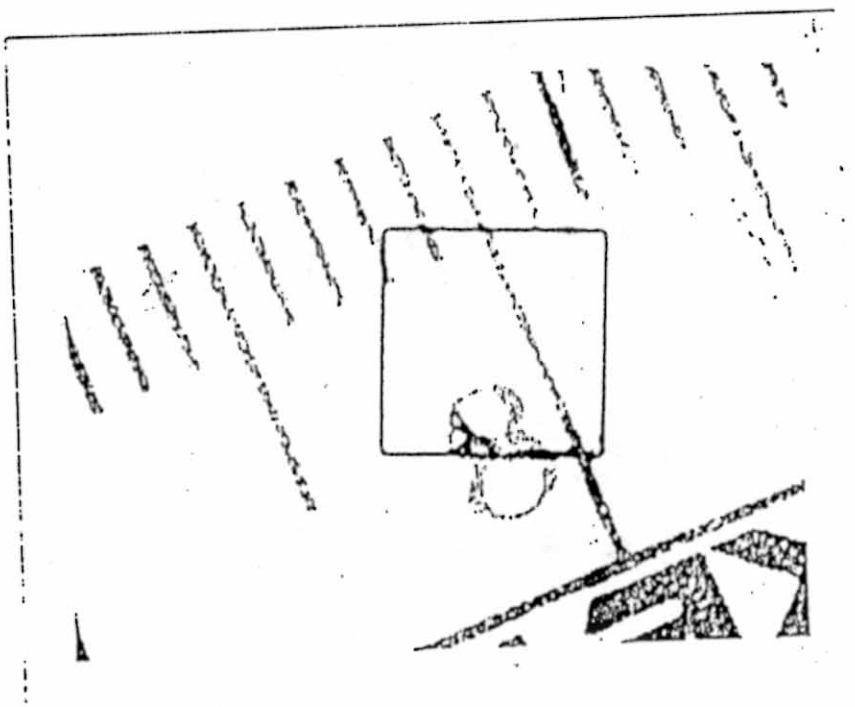

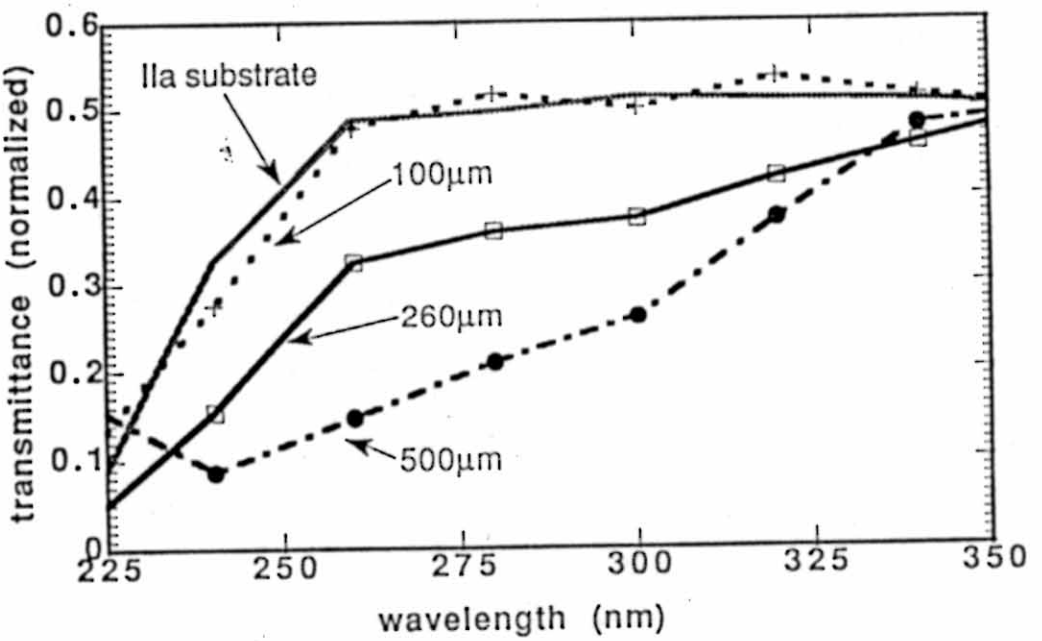
0.6
0.5
0.4
0.3
0.2
0.1
0
transmittance (normalized)
IIa substrate
100μm
260μm
500μm
225
250
275
300
325
350
wavelength (nm)

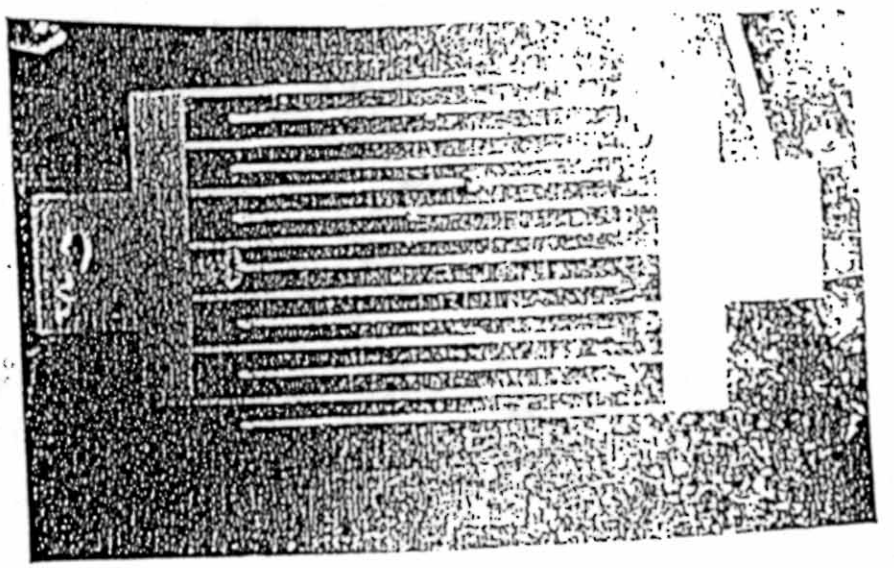

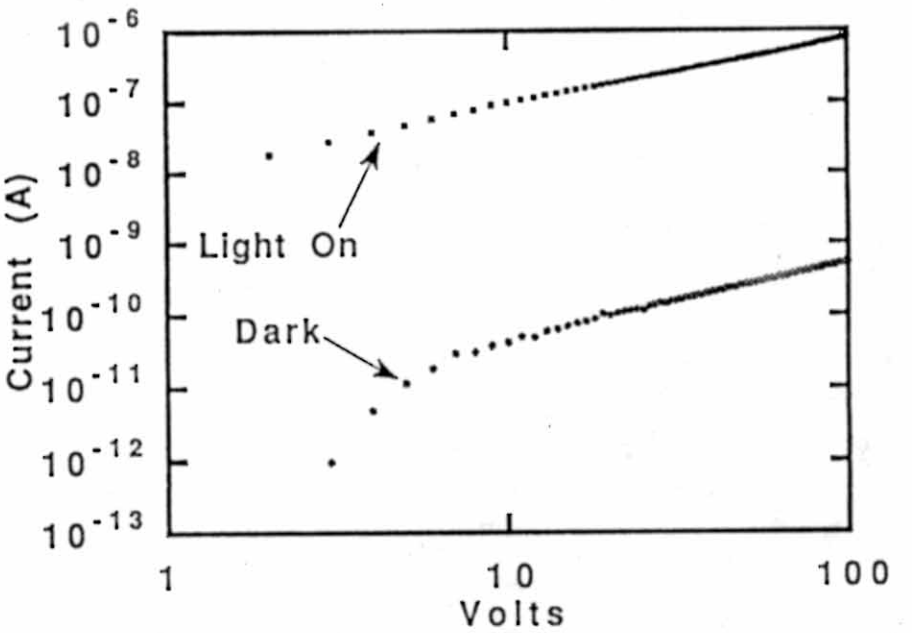
Current (A)
10-6
10-7
10-8
10-9
10-10
10-11
10-12
10-13
Light On
Dark
1
10
100
Volts

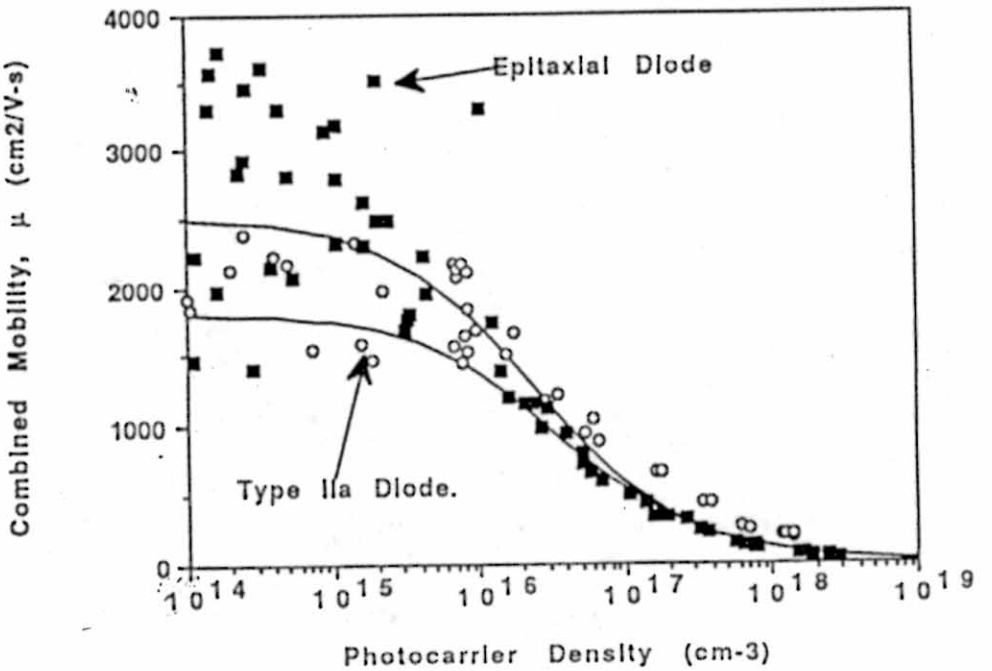
Combined Mobility, μ (cm2/V-s)
4000
3000
2000
1000
0
Epitaxial Diode
Type IIa Diode.
10^14
10^15
10^16
10^17
10^18
10^19
Photocarrier Density (cm-3)

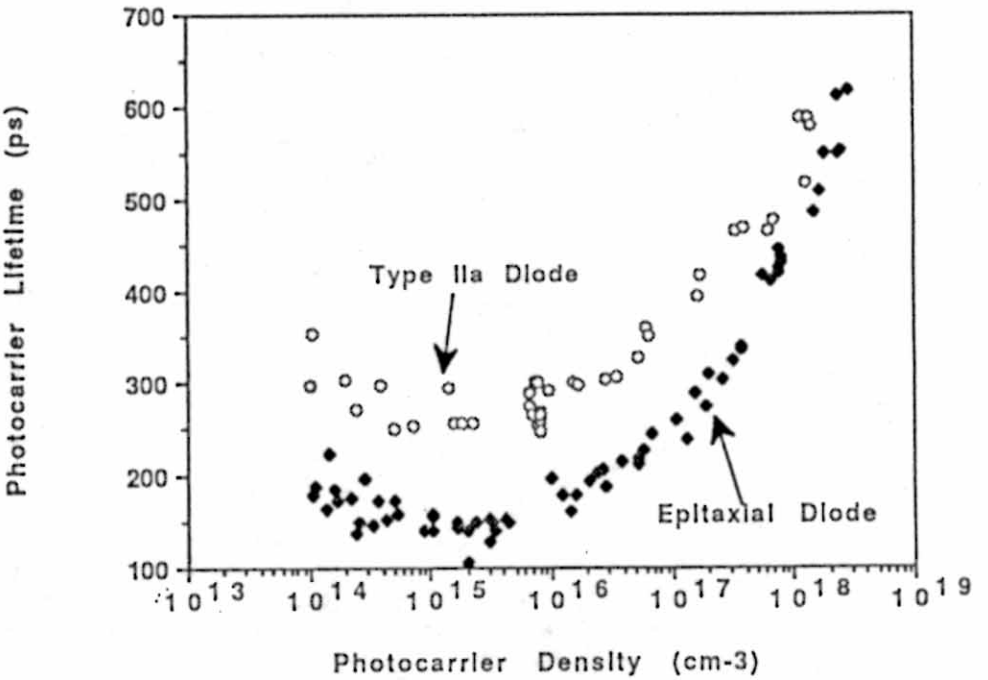
Photocarrier Lifetime (ps)
700
600
500
400
300
200
100
Type IIa Diode
Epitaxial Diode
10^{13}
10^{14}
10^{15}
10^{16}
10^{17}
10^{18}
10^{19}
Photocarrier Density (cm-3)

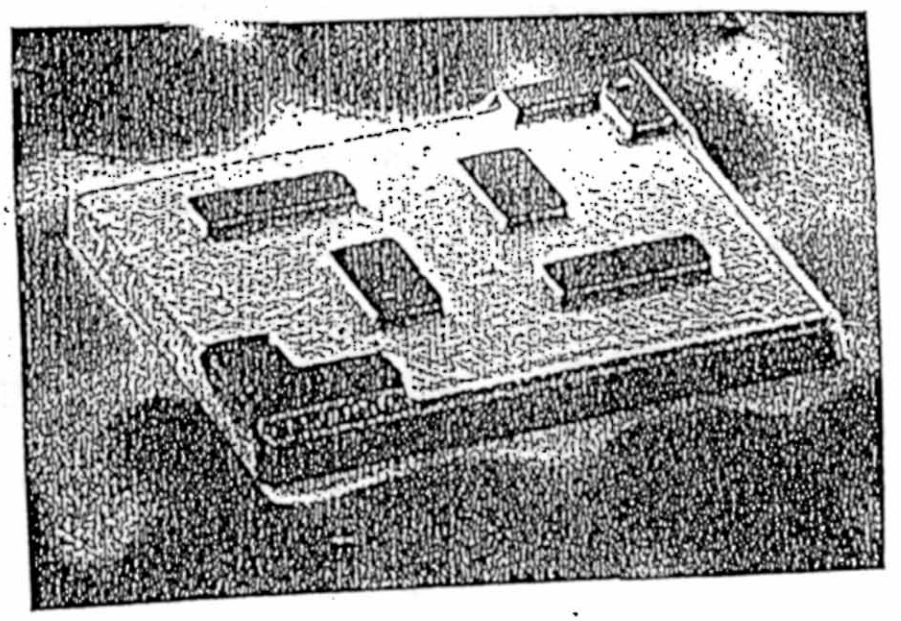

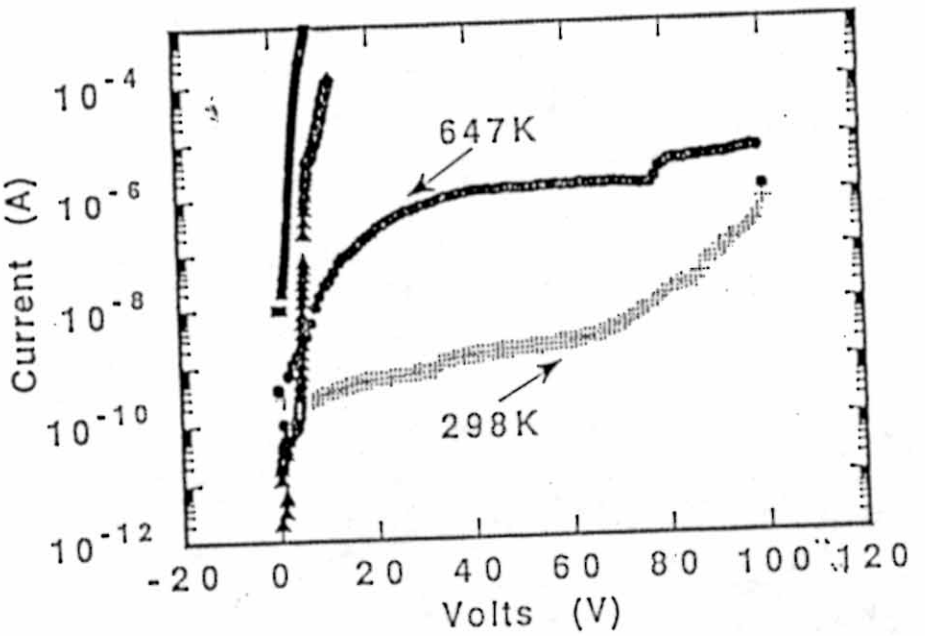
Current (A)
10-4
10-6
10-8
10-10
10-12
647K
298K
-20
0
20
40
60
80
100
120
Volts (V)